



# Interaction of Oxygen with the Stable $\text{Ti}_5\text{Si}_3$ Surface

Lora S. Chumakova <sup>1</sup>, Alexander V. Bakulin <sup>1,\*</sup> , Stephen Hocker <sup>2</sup>, Siegfried Schmauder <sup>2</sup>   
and Svetlana E. Kulkova <sup>1,3</sup>

- <sup>1</sup> Institute of Strength Physics and Materials Science, Siberian Branch of Russian Academy of Sciences, pr. Akademicheskoy 2/4, 634055 Tomsk, Russia; chumakova.lora@mail.ru (L.S.C.); kulkova@ms.tsc.ru (S.E.K.)  
<sup>2</sup> Institute for Materials Testing, Materials Science and Strength of Materials, University of Stuttgart, Pfaffenwaldring 32, 70569 Stuttgart, Germany; stephen.hocker@imwf.uni-stuttgart.de (S.H.); siegfried.schmauder@imwf.uni-stuttgart.de (S.S.)  
<sup>3</sup> Physics Department, National Research Tomsk State University, pr. Lenina 36, 634050 Tomsk, Russia  
\* Correspondence: bakulin@ispms.tsc.ru; Tel.: +7-3822-286-952

**Abstract:** The atomic structure and surface energies of several low-index surfaces (0001),  $(1\bar{1}00)$  and  $(11\bar{2}0)$  of  $\text{Ti}_5\text{Si}_3$  in dependence on their termination were calculated by the projector augmented-wave method within the density functional theory. It was revealed that the mixed TiSi-terminated (0001) surface is stable within the wide range of change in the Ti chemical potential. However, the Ti-terminated  $\text{Ti}_5\text{Si}_3(0001)$  surface is slightly lower in energy in the Ti-rich limit. The oxygen adsorption on the stable  $\text{Ti}_5\text{Si}_3(0001)$  surface with TiSi termination was also studied. It was shown that the three-fold coordinated *F*1 position in the center of the triangle formed by surface titanium atoms is the most preferred for oxygen adsorption on the surface. The appearance of silicon as neighbors of oxygen in other considered *F*-positions leads to a decrease in the adsorption energy. The factors responsible for the increase/decrease in the oxygen adsorption energy in the considered positions on the titanium silicide surface are discussed.

**Keywords:** oxygen; adsorption; titanium silicides; electronic structure; first principles calculations; surface



**Citation:** Chumakova, L.S.; Bakulin, A.V.; Hocker, S.; Schmauder, S.; Kulkova, S.E. Interaction of Oxygen with the Stable  $\text{Ti}_5\text{Si}_3$  Surface. *Metals* **2022**, *12*, 492. <https://doi.org/10.3390/met12030492>

Academic Editor: Antonije Onjia

Received: 22 February 2022

Accepted: 12 March 2022

Published: 14 March 2022

**Publisher's Note:** MDPI stays neutral with regard to jurisdictional claims in published maps and institutional affiliations.



**Copyright:** © 2022 by the authors. Licensee MDPI, Basel, Switzerland. This article is an open access article distributed under the terms and conditions of the Creative Commons Attribution (CC BY) license (<https://creativecommons.org/licenses/by/4.0/>).

## 1. Introduction

The interest in silicides in the research community is connected with their increasing industrial applications. At the beginning of the 1980s, the large scale production of silicon-based computers started. Silicides were used as ohmic contacts because of their low electrical resistivity and thermal compatibility with silicon [1,2]. It was found that disilicides such as  $\text{TiSi}_2$ ,  $\text{CoSi}_2$ ,  $\text{WSi}_2$ , etc., exhibit the most useful properties, and therefore most researches were focused on these compounds [1–5]. These researches included first of all oxidation behavior, which is very important in the photolithographic and thermal processing of circuits, atomic diffusivity to predict chemical reactivity of circuits and also the nature of chemical bonding in silicides, in order to understand the electrical and mechanical properties of materials. Other areas of research were spawned by the limitation of metallic alloys for structural applications at high temperatures. It is well known that superalloys, which are used in these applications, rapidly lose their resistance to creep and oxidation above 1100 °C [6]. Thus, the development of structural materials that can be used above this temperature is a main task of modern materials science. The criteria for materials for high temperature applications were formulated in the middle of the last century [7–11]. They include good creep and oxidation resistance above 1000 °C, low density, retention of strength at elevated temperatures and alloying or compositing possibilities to improve the ambient temperature brittleness inherent to most intermetallics. In this regard, aluminides and silicides seem to be most promising. Very important aspects of synthesizing these materials have also been established. In particular, it was revealed that alloying additions,

even in very small amounts, may significantly affect their properties [12–14]. Moreover, the processing route plays an essential role.

The electronic, mechanical, interfacial and diffusion properties of titanium aluminides were discussed in many works [6,15–22] including ours [23–27]. It is believed that the improvement in oxidation resistance of TiAl-based alloys can be reached by the addition of alloying elements, such as V, Nb, Ta, Y, B, W, Mo and Si, which allows the formation of a protective scale on the alloy surface or to slow down the oxygen diffusion rate. It was shown by a theoretical method that a silicon impurity promotes an increase in Ti-antistructural atoms in the  $\gamma$ -TiAl [28]. The authors of [16] think that the smart introduction and synergy of Si and Nb in the TiAl alloy present an attractive solution for high temperature applications. In this case the  $\text{Ti}_5\text{Si}_3$ ,  $\text{Al}_2\text{O}_3$  and  $\text{Nb}_2\text{Al}$  phases occur simultaneously at a sintering temperature of 1350 °C. It should be noted that  $\text{Ti}_5\text{Si}_3$  is formed as intermediate layers at the oxide–TiAl interface. The information about formation of  $\text{Nb}_2\text{Al}$  phase is contradictory. In particular, the formation of Nb aluminides was not observed in [29] in contrast to [16]. It should be noted that earlier in [30], it was also shown that the formation of  $\text{Ti}_5\text{Si}_3$  film and Al-rich layers leads to the formation of  $\text{Al}_2\text{O}_3$ , which suppresses TiAl alloy oxidation and is beneficial to oxidation resistance.

It is necessary to note that  $\text{Ti}_5\text{Si}_3$  itself is considered a promising candidate for high temperature applications due to its high melting point (2130 °C), high strength, low density and good creep resistance [31–36]. However, the major challenges of  $\text{Ti}_5\text{Si}_3$  applications include the difficulty of synthesis above 1600 °C, poor high temperature oxidation resistance and low fracture toughness. An addition of the second phase ( $\alpha$ - $\text{Al}_2\text{O}_3$ ,  $\text{ZrO}_2$ ,  $\text{Y}_2\text{O}_3$ , etc.) in the titanium silicide allows the oxidation resistance to be enhanced because of the thermodynamic benefit of the second phase and the slow growth rate [29,32,37]. In general, researchers have studied numerous coating systems on the TiAl alloy, such as aluminide and silicide coatings [38]. Some coatings can raise the oxidation protection of TiAl alloys because of formation of a continuously protective  $\text{Al}_2\text{O}_3$  or  $\text{SiO}_2$  scale. However, interdiffusion between coatings and Ti–Al alloys leads to phase degradation at high temperature and, prematurely, coating failure. Recently, based on the high affinity between Si and Ti, in [38], a novel silicon–aluminizing diffusion coating on the  $\gamma$ -TiAl alloy was suggested. Authors demonstrated that the  $\text{Ti}_5\text{Si}_3$  diffusion barrier may restrain the interdiffusion between the silicon–aluminizing diffusion coating and substrate that leads to enhancement of the long-term oxidation resistance performance of the coating.

It should be noted that silicides with the  $\text{Me}_5\text{Si}_3$  stoichiometry have many advantages over other silicides. We note that the crystal structure is a hexagonal type ( $P6_3/mcm$ ) if  $\text{Me} = \text{Sc}, \text{Y}, \text{Ti}, \text{Mn}$  and a body-centered tetragonal type ( $I4/mcm$ ) for  $\text{Me} = \text{La}, \text{Nb}, \text{Ta}, \text{Cr}, \text{V}, \text{Mo}, \text{W}$ . In contrast to disilicides, silicides with the  $\text{Me}_5\text{Si}_3$  composition have substantial alloying possibilities. For example, the hexagonal structure can accommodate up to 11 at.% of small interstitial atoms such as B, C, O or N.

Thus, as follows from this brief description, the study of the oxygen interaction with silicides or their surfaces can be useful for understanding of the mechanism of oxygen sorption and diffusion. The goal of the present paper is to study, at the microscopic level, the  $\text{Ti}_5\text{Si}_3$  surface stability and the mechanism of oxygen adsorption on the stable low-index surface.

## 2. Computational Details

The atomic and electronic structure of titanium silicide was calculated by the projector augmented-wave (PAW) method in the plane-wave basis [39,40] with the generalized gradient approximation for the exchange–correlation functional in the form of GGA–PBE [41]. The maximum energy of plane waves from the basic set was 550 eV. Convergence was considered achieved if the difference in total energies for the next two iterations did not exceed  $10^{-5}$  eV.

To calculate the energy of the  $\text{Ti}_5\text{Si}_3$  low-index surfaces with different orientations, the approach of multilayer symmetric films separated by a vacuum gap of at least 15 Å was

used. The relaxation of the atomic positions of the surface layers was carried out using conjugate gradient algorithm until the forces on atoms were less than 0.01 eV/Å. In the case of the (0001) surface, a  $\Gamma$ -centered grid of  $7 \times 7 \times 1$   $k$ -points was used, while grids of  $7 \times 9 \times 1$  and  $9 \times 5 \times 1$   $k$ -points, generated by the Monkhorst–Pack method [42] were used for the calculation of (1 $\bar{1}$ 00) and (11 $\bar{2}$ 0) surfaces, respectively.

Surface energy was calculated using the conventional equation of

$$\sigma = \frac{1}{2S} \left[ E_{\text{tot}}^{\text{slab}} - \frac{1}{3} N_{\text{Si}} \mu_{\text{Ti}_5\text{Si}_3}^{\text{bulk}} - \mu_{\text{Ti}}^{\text{bulk}} \left( N_{\text{Ti}} - \frac{5}{3} N_{\text{Si}} \right) - \Delta \mu_{\text{Ti}} \left( N_{\text{Ti}} - \frac{5}{3} N_{\text{Si}} \right) \right] \quad (1)$$

where  $N_{\text{Ti}}$  and  $N_{\text{Si}}$  are the number of titanium and silicon atoms in the silicide film, respectively,  $\mu_{\text{Ti}_5\text{Si}_3}^{\text{bulk}}$  is the chemical potential of the bulk silicide and  $\Delta \mu_{\text{Ti}}$  is the deviation of the titanium chemical potential on the  $\text{Ti}_5\text{Si}_3$  surface from its value in bulk titanium ( $\mu_{\text{Ti}}^{\text{bulk}}$ ), which can vary in the range of  $-\Delta H \leq \Delta \mu_{\text{Ti}} \leq 0$ , where  $\Delta H$  is the formation enthalpy of  $\text{Ti}_5\text{Si}_3$ ;  $\Delta H = 73.13$  kJ/mole of atoms (6.063 eV/f.u.). The calculated value of  $\Delta H$  agrees well with the experimental data (from  $72.5 \pm 0.8$  to  $78.1 \pm 5$  kJ/mole of atoms [43–45] and references therein) and theoretical values (6.01 eV/f.u. [46], 6.16 eV/f.u. [47], 6.38 eV/f.u. [48]). More details of the calculation of surface energy are given in our earlier work, e.g., [49].

Adsorption of oxygen on the surface was studied in the model of asymmetric films as was described in [23,49,50] in the case of titanium aluminides. Atoms of the three layers on the underside of the film were fixed in bulk positions, while the positions of the atoms of the remaining layers were optimized. The adsorption energy of an oxygen atom was calculated by the equation

$$E_{\text{ads}} = -[E_{\text{O/Ti}_5\text{Si}_3} - E_{\text{Ti}_5\text{Si}_3} - 1/2E_{\text{O}_2}] \quad (2)$$

where  $E_{\text{O/Ti}_5\text{Si}_3}$  and  $E_{\text{Ti}_5\text{Si}_3}$  are the total energies of the surface with oxygen and without it, and  $E_{\text{O}_2}$  is the total energy of an oxygen molecule, calculated in an empty cell with dimensions  $12 \times 12 \times 12$  Å.

### 3. Results and Discussion

#### 3.1. Surface Stability

The intermetallic compound  $\text{Ti}_5\text{Si}_3$  has hexagonal structure  $D8_8$  and space group  $P6_3/mcm$  (№ 193) as was mentioned earlier. Titanium atoms occupy two types of Wyckoff positions:  $4d$  (1/3, 2/3, 0) and  $6g$  (0.250, 0, 1/4), whereas silicon atoms are located at the  $6g$  (0.608, 0, 1/4) positions (Figure 1a). Theoretical lattice parameters ( $a = 7.466$  Å and  $c = 5.108$  Å) differ from experimental ones [51] by less than 0.8%. We consider the following low-index surfaces: (0001), (1 $\bar{1}$ 00) and (11 $\bar{2}$ 0), which are shown in Figure 1b.

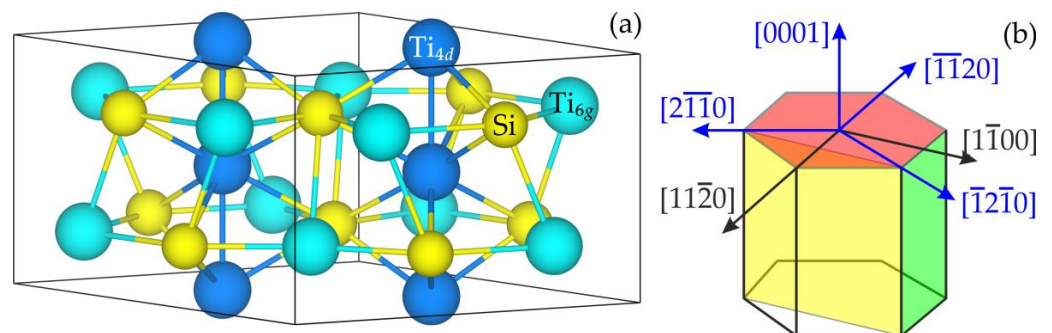


**Figure 1.** Atomic structure of bulk  $\text{Ti}_5\text{Si}_3$  (a) and denotation of low-index crystallographic planes in the hexagonal cell (b).

Figure 2 demonstrates the atomic structure of the three examined surfaces of  $\text{Ti}_5\text{Si}_3$ . The (0001) surface has two terminations: it can be the mixed TiSi-terminated surface with  $\text{Ti}_{6g}$  and Si atoms in the surface layer in the ratio 1:1 and the Ti-terminated one with  $\text{Ti}_{4d}$

atoms in the surface layer (Figure 2a). In the case of  $(1\bar{1}00)$  and  $(11\bar{2}0)$  surfaces there are seven and six surface terminations, respectively (Figure 2b,c). They can be terminated by titanium, silicon or mixed atomic layers. In the latter case, the surface layer is formed by the same number of titanium and silicon atoms.

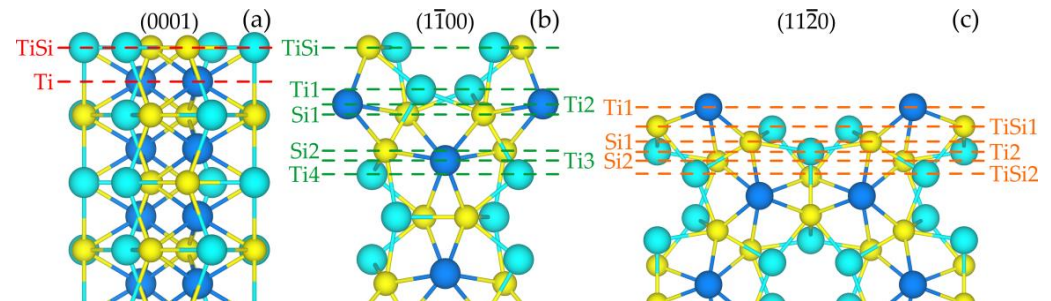


**Figure 2.** Atomic structure of the low-index surfaces (a) (0001), (b)  $(1\bar{1}00)$  and (c)  $(11\bar{2}0)$  (side view) of the compound  $\text{Ti}_5\text{Si}_3$ .

Figure 3 presents the calculated diagram of stability for considered surfaces of  $\text{Ti}_5\text{Si}_3$ . It is seen that the Ti-terminated (0001) surface is stable in the Ti-rich limit, while for other values of the chemical potential of titanium, the lowest surface energy corresponds to the (0001) surface with a mixed TiSi termination. However, the difference in the surface energies of both structures in the Ti-rich limit is only  $0.02 \text{ J/m}^2$ . In the Si-rich limit, the corresponding surface energy of the TiSi-terminated (0001) surface is  $1.62 \text{ J/m}^2$ , which agrees well with the experimental value of  $1.675 \text{ J/m}^2$  [52].

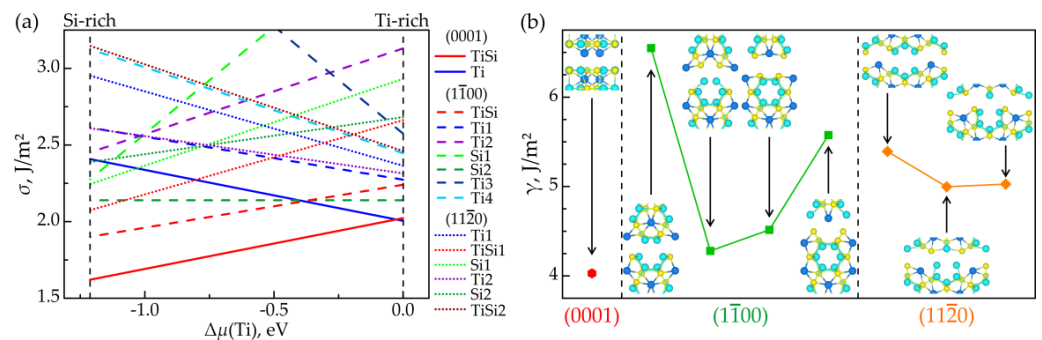


**Figure 3.** Dependence of surface energies of low-index surfaces of  $\text{Ti}_5\text{Si}_3$  on the chemical potential of titanium (a); cleavage energy (in  $\text{J/m}^2$ ) for corresponding planes shown by solid lines (b).

It should be noted that the mixed TiSi termination of the  $(1\bar{1}00)$  surface, has the lowest energy in a wide range of  $\Delta\mu_{\text{Ti}}$ , while in the Ti-rich limit the Si2-terminated surface is lower in energy. As seen from Figure 2b, such terminations can be obtained in the case of cleavage along the largest interlayer distances. A mixed TiSi1-terminated  $(11\bar{2}0)$  surface has lower energy in the Si-rich limit, whereas the Ti2-terminated surface is stable in the Ti-rich region. Several words should be said about temperature effect on the surface energy calculations. It is known that such corrections are usually neglected in calculations because they do not almost influence relative values of surface energies. Taking into account vibrational entropy, our corrections of the surface energy were less than  $\sim 0.07 \text{ J/m}^2$ . Since the  $(0001)_{\text{TiSi}}$  surface lies substantially lower than other surfaces, shown in Figure 3a, we can conclude that this correction does not influence the obtained trends.

The calculations of the cleavage energies for several planes shown in Figure 3b allows the conclusion to be made that the basal plane is more preferred for mechanical failure. It is to be noted that the cleavage energy is defined as the energy per area required to separate a crystal into two parts. In accordance with the Dupré equation with zero interfacial energy it can be estimated as

$$\gamma = \sigma_1 + \sigma_2 \quad (3)$$

where  $\sigma_1$  and  $\sigma_2$  are the surface energies of the formed surfaces.

Since the lattice parameter of  $\text{Ti}_5\text{Si}_3$  corresponds to  $a = b > c$ , then, in accordance with the classical crystal growth theory [53], the  $\text{Ti}_5\text{Si}_3$  growth rate along the  $\langle 0001 \rangle$  direction is higher than that of other directions and titanium silicide tends to grow in the form of a hexagonal prism. Since  $\sigma(0001) < \sigma(1\bar{1}00) < \sigma(11\bar{2}0)$ , the side faces of this prism are formed by the  $\{1\bar{1}00\}$  planes. The conclusion about the crystal growth mechanism agrees with the experiment [54].

Table 1 shows the relaxations of the first three interlayer distances, as well as the splitting of the mixed surface layer for the four surfaces with the lowest surface energy. The relaxation of interlayer distances was estimated by the formula  $\Delta d_{ij} = (d_{ij} - d_0)/d_0$ , where  $d_0$  is the interplanar distance in the bulk, and  $i, j$  are the numbers of the corresponding atomic layers. Since the titanium and silicon atoms in the mixed layers are slightly displaced, their average position was used to estimate the surface relaxation. It is seen that the stable surface demonstrates the strongest relaxation of the interlayer distances: the compression of the first interlayer distance reaches 19.6%. In this case, the relaxation has an alternating character and decays very quickly into bulk. For the Ti-terminated (0001) surface,  $d_{12}$  is almost unchanged, while  $\Delta d_{23}$  and  $\Delta d_{34}$  are the opposite in sign in respect to the previous mixed layer terminated surface. In the case of the TiSi-terminated ( $1\bar{1}00$ ) surface, the second interlayer distance  $d_{23}$  changes less than  $d_{34}$ . Irrespective of the surface orientation, in the case of a mixed terminated surface, the silicon atoms are located above the titanium atoms ( $\varepsilon > 0$  in Table 1).

**Table 1.** Relaxation of the first ( $\Delta d_{12}$ ), the second ( $\Delta d_{23}$ ) and the third ( $\Delta d_{34}$ ) interlayer distances for pure  $\text{Ti}_5\text{Si}_3$  surfaces and splitting  $\varepsilon$  of the first layer.

Surface	(0001)		(1–100)	
Termination	TiSi	Ti	TiSi	Si2
$\Delta d_{12}$ , %	−19.6	−0.1	−3.3	−3.3
$\Delta d_{23}$ , %	+13.7	−5.9	+0.5	−4.7
$\Delta d_{34}$ , %	−0.9	+4.5	+5.5	+1.9
$\varepsilon$ , Å	0.19	–	0.12	–

### 3.2. Oxygen Adsorption

The adsorption positions of oxygen on the  $\text{Ti}_5\text{Si}_3(0001)_{\text{TiSi}}$  surface are shown in Figure 4. We denote the positions at the center of the triangles formed by the surface (subsurface) atoms as  $F$ ; a bridge position between two surface atoms— $B$ ; the top positions above the Ti (Si) atoms of the surface layer— $T_{\text{Ti}}$  ( $T_{\text{Si}}$ ); the positions above the Ti subsurface atom— $T2_{\text{Ti}}$ .

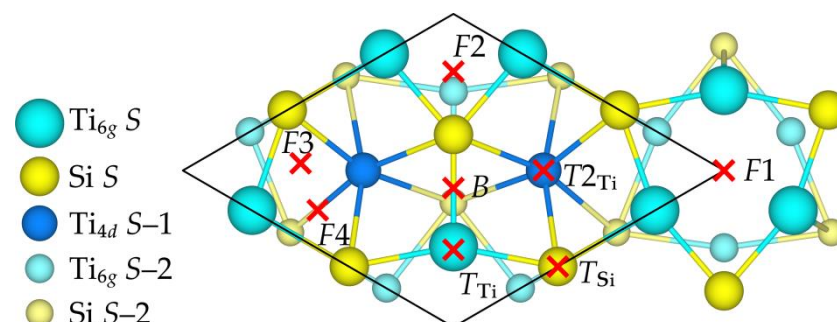


**Figure 4.** Positions of oxygen adsorption on the  $\text{Ti}_5\text{Si}_3(0001)_{\text{TiSi}}$  surface.

It can be seen from Table 2 that the most preferred position is  $F1$ , where oxygen interacts with three surface titanium atoms. In this case, the O–Ti bond length is 1.96 Å as in the case of  $\text{TiO}_2$  with a rutile structure. The adsorption energy in the  $F2$  position is  $\sim 0.8$  eV lower than in the  $F1$  position (Table 2). In this case, the oxygen atom interacts with

two Ti and one Si surface atoms. Almost the same adsorption energies were calculated for *F3* and *F4* positions. These sites are very similar (oxygen interacts with two Ti of surface and subsurface atoms and one Si surface atom) and the difference is connected with atoms in the third layer from the surface. A decrease in the adsorption energies in the *F3* and *F4* positions is due to the increase in O–Ti bond length by 0.04–0.2 Å. The latter leads to a decrease in the covalent contribution to the chemical bond in comparison with the *F1* position. In addition, the ionic contribution in the chemical bond decreases almost twice (Table 2).

**Table 2.** Adsorption energy of oxygen ( $E_{\text{ads}}$ ) on the  $\text{Ti}_5\text{Si}_3(0001)_{\text{TiSi}}$  surface, distance between oxygen and the nearest atoms of the substrate ( $d(\text{O}-\text{X})$ ), height of oxygen relative to the surface layer ( $h$ ), charge transfer to oxygen atom ( $Q$ ) and overlap population for O–X bonds ( $\theta$ ).

Position	<i>F1</i>	<i>F2</i>	<i>F3</i>	<i>F4</i>	<i>B</i>	<i>T2</i> <sub>Ti</sub>
$E_{\text{ads}}$ , eV	6.13	5.30	4.06	4.15	3.87	2.00
$d(\text{O}-\text{Ti}_{6\text{gi}} \text{S})$ , Å	1.96	1.97	2.00	1.96	1.86	2.95
$d(\text{O}-\text{Si} \text{S})$ , Å	3.15	1.90	1.71	1.71	1.71	2.52
$d(\text{O}-\text{Ti}_{4\text{d}} \text{S}-1)$ , Å	4.74	3.80	2.13	2.17	3.28	1.86
$h$ , Å	0.91	0.93	0.60	0.61	1.02	0.71
$Q^{\text{DDEC6}}$ , el.	0.76	0.48	0.38	0.36	0.35	0.35
$\Sigma\theta$ , el.	1.65	1.51	1.49	1.50	1.43	1.31
$\theta(\text{O}-\text{Ti}_{6\text{g}} \text{S})$ , el.	0.48	0.43	0.37	0.41	0.52	0.05
$\theta(\text{O}-\text{Si} \text{S})$ , el.	0.07	0.65	0.86	0.85	0.87	0.23
$\theta(\text{O}-\text{Ti}_{4\text{d}} \text{S}-1)$ , el.	0.00	0.00	0.26	0.24	0.02	0.47

Among the considered bridge sites only one position, shown in Figure 4, was found to be stable; however,  $E_{\text{ads}}$  is 2.26 eV lower than in the *F1* position. The explanation is almost the same as was given above. In the *T2*<sub>Ti</sub> site, oxygen forms a chemical bond only with the *Ti*<sub>4d</sub> subsurface atom. It should be noted that both *T* positions above surface atoms are unstable and oxygen moves to the neighboring *F1* and *F2* sites. The preference of the Ti-rich positions for oxygen adsorption found on the  $\text{Ti}_5\text{Si}_3(0001)$  surface correlates with the trend established for Ti–Al alloys in our earlier papers [23,48]. As was shown in the experimental paper [55], titanium oxide scale grows on  $\text{Ti}_5\text{Si}_3$  surface at the initial oxidation stage.

Several remarks should be made in connection with the calculation of oxygen adsorption energies. It is necessary to emphasize that in reality,  $\text{O}_2$  adsorption on the  $\text{Ti}_5\text{Si}_3$  surface takes place. Nevertheless, our test calculations show that after adsorption of  $\text{O}_2$  in any position, its dissociation occurs and oxygen atoms can easily diffuse on the surface to occupy positions with the highest binding energy. Thus, there is no reason to simulate  $\text{O}_2$  molecule adsorption on the surface as in [56]. The second remark is connected with thermodynamic corrections of adsorption energy. It is well known that direct simulation of high temperature oxidation of the material surface is difficult in the framework of the density functional theory. However, the methods, which give information for the ground state of material, are intensively used to study the adsorption of oxygen. It is believed that in order to understand the mechanisms of the surface oxidation, it is necessary to identify the main tendencies of the interaction of oxygen with the atoms in the surface layers, which are determined by the electronic subsystem and are weakly dependent on temperature. Using the approach described in paper [57], it is possible to show that the Gibbs free adsorption energy reaches ~3 eV at high temperature and moderate oxygen partial pressure, but the difference in these energies for considered sites is almost the same as that in the adsorption energies in Table 2. This is a reason to neglect this effect in most investigations of oxygen adsorption on metallic surfaces.

As can be seen from Table 2, there is a correlation between the values of oxygen adsorption energy in considered positions and charge transfer ( $Q$ ) to the adatom (the ionic contribution to chemical bond). In particular, in the *F1* position, the charge transfer from the substrate to the oxygen atom reaches the maximum value of 0.76 el., if the DDEC6 (Density

Derived Electrostatic and Chemical) method [58] is used in its estimation. The charge density difference distribution (Figure 5a) demonstrates the charge depletion region near Ti surface atoms and its accumulation around oxygen. In the *F2* position, the appearance of the silicon in the nearest neighbors of oxygen lowers the adsorption energy by  $\sim 0.8$  eV. At the same time, the charge transfer to oxygen decreases by a factor of 1.6. Figure 5b demonstrates a wider area of charge density depletion near the silicon atom than that near Ti atoms. Indeed, our estimation reveals that the silicon atom loses 0.38 el., whereas the titanium atom only loses 0.09 el. It was 0.27 el. in the previous case of the *F1* position. We note that charge transfer depends strongly on the method of its estimation. As was mentioned above, in the present paper the results obtained by the DDEC6 method are discussed. A decrease in the charge transfer to the oxygen atom in the *F2* position is also accompanied by an insignificant decrease in the overlap population ( $\theta$ ) of oxygen bonds with surface atoms. It is necessary to point out that  $\theta$  reflects the covalent contribution to the mechanism of chemical bonding. The overlap population is also estimated by the DDEC6 method [59].

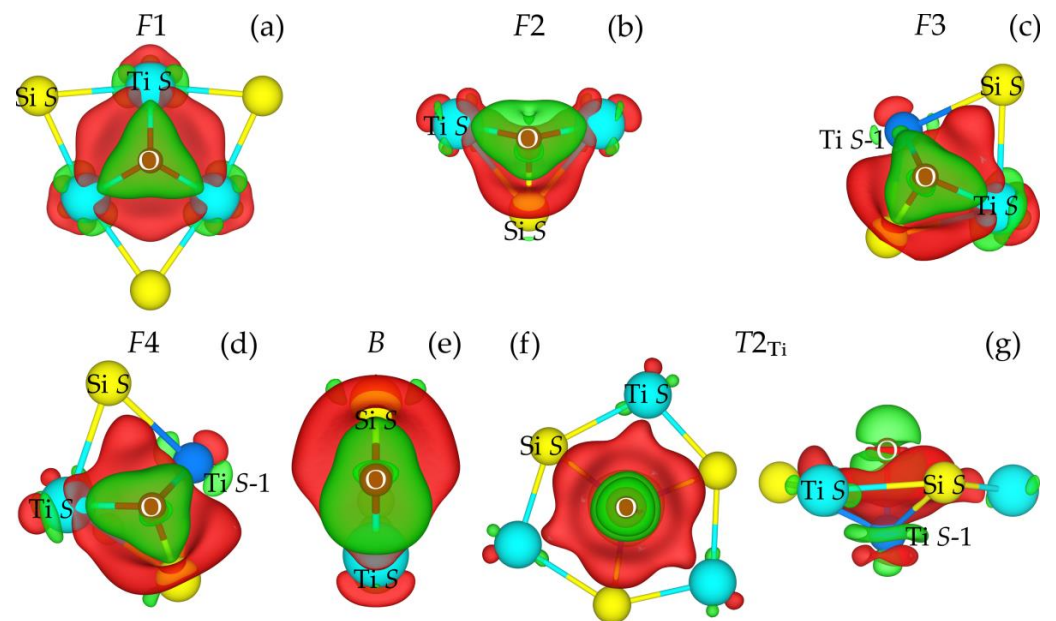


**Figure 5.** Distribution of charge density difference ( $\Delta\rho = \rho_O + \rho_{\text{Ti}_5\text{Si}_3} - \rho_{\text{O}/\text{Ti}_5\text{Si}_3}$ ) for  $\text{Ti}_5\text{Si}_3(0001)_{\text{TiSi}}$  surface with oxygen adsorbed in *F1* (a), *F2* (b), *F3* (c), *F4* (d), *B* (e), *T2*<sub>Ti</sub> (f,g). Top view (a–f) and side view (g) are given. Charge depletion and accumulation regions are shown by red and green colors, respectively.

In the *F3* and *F4* positions, the oxygen obtains an even smaller charge, which leads to a subsequent decrease in  $E_{\text{ads}}$ , although the overlap population remains practically unchanged. In this case the charge transfer from the subsurface Ti atom is almost absent, which can be seen in Figure 5c,d. Despite the decrease in the coordination of the oxygen atom in the *B* and *T2*<sub>Ti</sub> positions, the charge transfer remains almost the same as in the *F3* and *F4* positions, but the overlap population decreases by 0.1–0.2 el. It should be noted that in the *B* position, oxygen actively interacts with the silicon atom since its *s,p*-electrons are more easily involved in the interaction than Ti *d*-electrons (Figure 5e). The lowest adsorption energy in the *T2*<sub>Ti</sub> position is connected with the fact that Ti- $d_{z^2}$  orbitals are practically unoccupied, while the O–Ti bond length is the smallest (1.86 Å) among considered oxygen adsorption positions. In this case, the polarization of Ti orbitals is all that occurs. That leads to a small contribution of this mechanism in the chemical bonding. At the same time, the charge transfer is only due to the nearest silicon surface atoms. This is clearly seen in Figure 5f.

The fact that specific positions on the titanium silicide surface are more preferable for the oxygen adsorption can be explained by analyzing the local densities of states (DOS) of oxygen and the nearest titanium and silicon atoms, which are shown in Figure 6 for all considered positions. Since oxygen predominantly interacts with atoms of the surface layer, this leads to the appearance of peaks on Ti and Si local DOSs, which coincide in the energy with the corresponding peaks of O *s,p*-bands. Since the sharp peak corresponding to the O *s*-band is located at  $-19$  eV, it is not shown in Figure 6. It can be seen that in the F1 position, the narrow O *p*-band is split and its minimum locates at  $-5$  eV. A small double peak of the  $Ti_{6g}$  states is also located at the same energies (Figure 6a). It is split off from the Ti valence band bottom because of its interaction with the O *p*-states, and a pseudogap is formed between the titanium states at energy of  $-4$  eV.

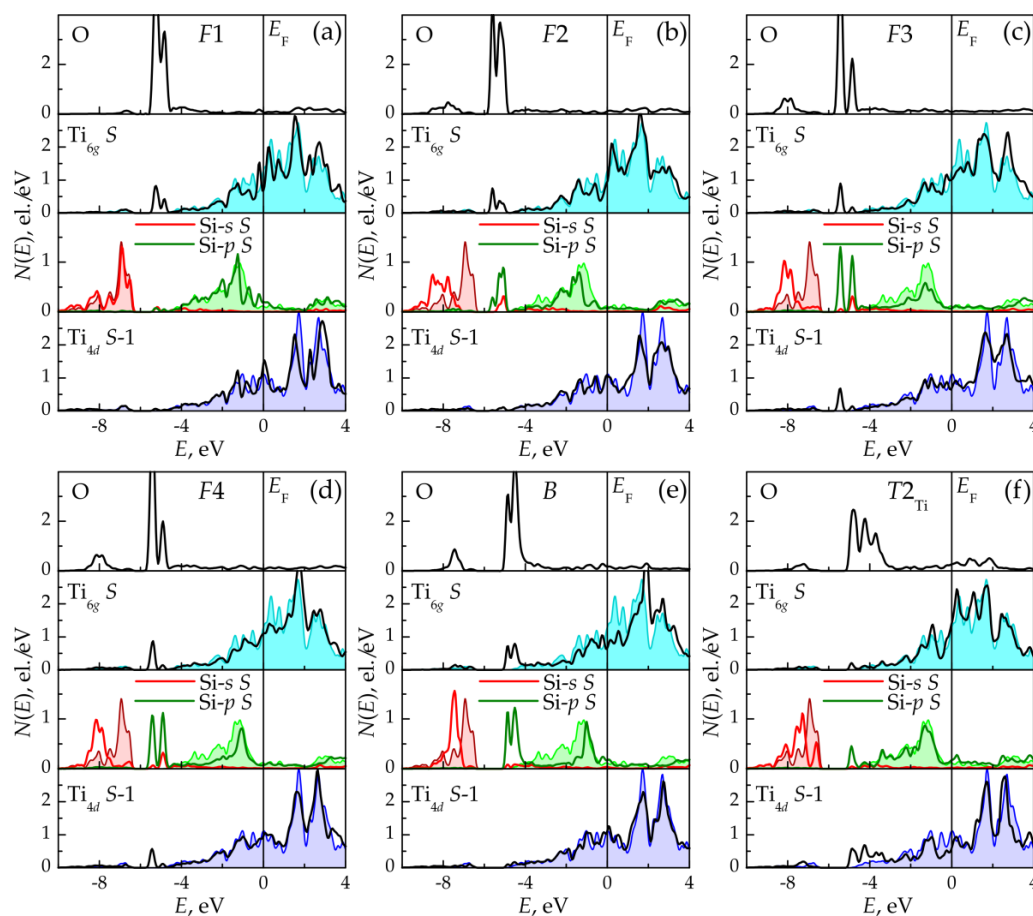


**Figure 6.** Local DOS of oxygen and the nearest atoms of the surface (S) and subsurface (S-1) layers for all positions: (a) F1, (b) F2, (c) F3, (d) F4, (e) B and (f)  $T2_{Ti}$ . Local DOS of Ti and Si atoms on the clean surface are shown in color fill.

The local DOS of the surface silicon atom is less changed. There is only a small peak which is split off from the Si *p*-band, but it appears because of the hybridization of Si *p*-orbitals with Ti *s,d*-orbitals. With the latter, oxygen is directly bound to the surface, rather than due to direct interaction with the surface silicon since the O-Si interatomic distance is  $3.15$  Å. The local DOS of the  $Ti_{4d}$  atom is also almost unchanged since the O-Ti distance of  $4.74$  Å is larger than the sum of their atomic radii. A small peak of the subsurface  $Ti_{4d}$  DOS at  $-6.8$  eV is also a result of indirect interaction with oxygen due to hybridization with the Si orbitals of surface atoms. In general, the appearance of new peaks, the change in the structure of the local DOS curves of the surface and subsurface Ti and Si atoms, their shift in energy relative to the DOS of corresponding atoms on a clean surface and the splitting of low-lying states indicate the formation of new Ti(Si)-O bonds and the weakening of



chemical bonds between the atoms of the surface and subsurface layers. The DOS of those atoms that are directly involved in the interaction with oxygen is changed most strongly. This behavior is also observed for other adsorption positions.

The structure of the O DOS in other *F*-positions changes insignificantly. The difference is in the stronger splitting of the main peak of the O *p*-band in the case of *F3* and *F4* positions (Figure 6c,d) and its shift towards the Fermi level in the case of *T2<sub>Ti</sub>* position (Figure 6f). In the latter case, the structure and width of the O *p*-band changes also. It is seen from Figure 6b–f that oxygen interacts strongly with Si surface atoms: the peak of Si *p*-DOS at the energies where the O *p*-band is located increases in magnitude. Moreover, the shift of the Si *s*-band towards negative energies is observed that leads to an increase in the O small peak at energy  $-8$  eV, which splits off from the main peak. In addition, Figure 6c,d shows that the DOS of a subsurface *Ti<sub>4d</sub>* atom changes to a greater degree than that in the case of O adsorption in the *F1* position. Moreover, one can see that this change in DOS of the subsurface *Ti<sub>4d</sub>* atom is expressed more strongly in comparison with DOS of the *Ti<sub>6g</sub>* atom because only the former one involves direct interaction with oxygen in the *T2<sub>Ti</sub>* position. Other atoms interact with oxygen indirectly due to hybridization with the *Ti<sub>4d</sub>* atoms.

#### 4. Conclusions

The paper presents the results of calculations of surface energies of several  $\text{Ti}_5\text{Si}_3$  low-index surfaces and oxygen adsorption on the stable surface performed by the projector augmented-wave method. It is revealed that the mixed TiSi-terminated  $\text{Ti}_5\text{Si}_3(0001)$  surface is stable for almost the whole range of changes in the titanium chemical potential. The Ti-terminated  $\text{Ti}_5\text{Si}_3(0001)$  surface is lower in energy in the Ti-rich limit, although the difference is only  $0.02 \text{ J/m}^2$ . It was obtained that for considered  $\text{Ti}_5\text{Si}_3$  surfaces, the following relationship is valid:  $\sigma(0001) < \sigma(1\bar{1}00) < \sigma(11\bar{2}0)$ . The calculation of the cleavage energy shows that the  $\text{Ti}_5\text{Si}_3$  mechanical failure occurs more easily along the (0001) plane.

It is shown that the adsorption of oxygen on the TiSi-terminated  $\text{Ti}_5\text{Si}_3(0001)$  surface is most preferred at the three-fold coordinated Ti-rich *F1* position, in which oxygen interacts with three surface titanium atoms. The presence of silicon as the neighbors of oxygen in other *F*-positions leads to a decrease in the adsorption energy due to a decrease in ionic and covalent contributions to chemical bonding of the oxygen atom with the substrate. The positions above surface atoms are found to be unstable. The adsorption energy above the subsurface Ti atom is the smallest because the orbitals that promote the oxygen–titanium interaction are almost unoccupied. In general, an increase in the oxygen adsorption energy is connected with an increase in the content of titanium in the nearest environment of oxygen. This indicates titanium oxide scale growth at the initial oxidation stage and is in agreement with the experiment.

Thus, in the present paper, the microscopic aspect of the oxygen interaction with the stable  $\text{Ti}_5\text{Si}_3(0001)$  surface is considered. Despite many factors, including temperature, structural transformations, etc., not being taken into account in the calculations; nevertheless, they allow estimation, quite correctly, of the adsorption and binding energies of oxygen on the surface and to obtain information on the initial stage of oxidation. The obtained results allow us to suggest the preferred pathway for oxygen diffusion from surface inside bulk materials. The adsorption of oxygen in the *F1* position leads to oxygen penetration in subsurface layers and its diffusion along the [0001] direction between octahedral sites. Actually, this is only a fast diffusion channel but it can be blocked by other small interstitial impurities such as boron. The investigation of oxygen diffusion in titanium silicide will be presented in our forthcoming paper.

**Author Contributions:** Conceptualization, A.V.B. and S.E.K.; methodology, S.E.K. and S.H.; software, A.V.B. and L.S.C.; validation, S.E.K. and S.H.; formal analysis, L.S.C.; investigation, A.V.B., L.S.C., S.E.K. and S.H.; data curation, S.E.K. and S.H.; writing—original draft preparation, A.V.B., S.E.K., S.H. and S.S.; writing—review and editing, S.E.K. and S.S.; visualization, A.V.B., L.S.C. and S.H.; supervision, S.E.K.; project administration, A.V.B. and S.E.K.; funding acquisition, S.E.K. All authors have read and agreed to the published version of the manuscript.

**Funding:** The work was supported by the Russian Science Foundation, project No. 22-23-00078.

**Data Availability Statement:** The data presented in this study are available on request from the corresponding author.

**Acknowledgments:** Numerical calculations were performed on the SKIF-Cyberia supercomputer at TSU.

**Conflicts of Interest:** The authors declare no conflict of interest.

## References

1. Gambino, J.P.; Colgan, E.G. Silicides and ohmic contacts. *Mater. Chem. Phys.* **1998**, *52*, 99–146. [[CrossRef](#)]
2. Chen, L.J. *Silicide Technology for Integrated Circuits*; The Institute of Engineering and Technology: London, UK, 2004; pp. 1–279.
3. Lie, L.N.; Tiller, W.A.; Saraswat, K.C. Thermal oxidation of silicides. *J. Appl. Phys.* **1984**, *56*, 2127–2132. [[CrossRef](#)]
4. Jeon, H.; Sukow, C.A.; Honeycutt, J.W.; Rozgonyi, G.A.; Nemanich, R.J. Morphology and phase stability of TiSi<sub>2</sub> on Si. *J. Appl. Phys.* **1992**, *71*, 4269–4276. [[CrossRef](#)]
5. La Via, F.; Mammoliti, F.; Corallo, G.; Migas, D.B.; Miglio, L. Formation of the TiSi<sub>2</sub> C40 as an intermediate phase during the reaction of the Si/Ta/Ti system. *Appl. Phys. Lett.* **2001**, *78*, 1864–1866. [[CrossRef](#)]
6. Li, Z.; Gao, W. High temperature corrosion of intermetallics. In *Intermetallics Research Progress*; Berdovsky, N., Ed.; Nova Science: New York, NY, USA, 2008; pp. 1–64.
7. Fleischer, R.L. High-strength, high-temperature intermetallic compounds. *J. Mater. Sci.* **1987**, *22*, 2281–2288. [[CrossRef](#)]
8. Anton, D.L.; Shah, D.M.; Duhl, D.N.; Giamei, A.F. Selecting high-temperature structural intermetallic compounds: The engineering approach. *JOM* **1989**, *9*, 12–17. [[CrossRef](#)]
9. Fleischer, R.L.; Dimiduk, D.M.; Lipsitt, H.A. Intermetallic compounds for strong high-temperature materials: Status and potential. *Annu. Rev. Mater. Sci.* **1989**, *19*, 231–263. [[CrossRef](#)]
10. Shah, D.M.; Berczik, D.; Anton, D.L.; Hecht, R. Appraisal of other silicides as structural materials. *Mater. Sci. Eng.* **1992**, *A155*, 45–57. [[CrossRef](#)]
11. Skrzypek, J.J.; Ganczarski, A.W.; Rustichelli, F.; Egner, H. Material properties for high temperature applications. In *Advanced Materials and Structures for Extreme Operating Conditions*; Springer: Berlin, Germany, 2008; pp. 1–12. [[CrossRef](#)]
12. Takasugi, T. Effects of alloying additions on intergranular fracture of ordered intermetallics. *Mater. Res. Soc. Symp. Proc.* **1991**, *213*, 403–416. [[CrossRef](#)]
13. Grabke, H.J.; Meier, G.H. Accelerated oxidation, internal oxidation, intergranular oxidation, and peeling of intermetallic compounds. *Oxid. Met.* **1995**, *44*, 147–176. [[CrossRef](#)]
14. Meyer, M.K.; Akinc, M. Oxidation behavior of boron-modified Mo<sub>5</sub>Si<sub>3</sub> at 800°–1300°C. *J. Am. Ceram. Soc.* **1996**, *79*, 938–944. [[CrossRef](#)]
15. Dai, J.; Zhu, J.; Chen, C.; Weng, F. High temperature oxidation behavior and research status of modifications on improving high temperature oxidation resistance of titanium alloys and titanium aluminides: A review. *J. Alloys Compd.* **2016**, *685*, 784–798. [[CrossRef](#)]
16. Gui, W.; Liang, Y.; Hao, G.; Lin, J.; Sun, D.; Liu, M.; Liu, C.; Zhang, H. High Nb-TiAl-based porous composite with hierarchical micro-pore structure for high temperature applications. *J. Alloys Compd.* **2018**, *744*, 463–469. [[CrossRef](#)]
17. Shanabarger, M.R. Comparative study of the initial oxidation behavior of a series of titanium–aluminum alloys. *Appl. Surf. Sci.* **1998**, *134*, 179–186. [[CrossRef](#)]
18. Koizumi, Y.; Kishimoto, M.; Minamino, Y.; Nakajima, H. Oxygen diffusion in Ti<sub>3</sub>Al single crystals. *Philos. Mag.* **2008**, *88*, 2991–3010. [[CrossRef](#)]
19. Song, Y.; Xing, F.J.; Dai, J.H.; Yang, R. First-principles study of influence of Ti vacancy and Nb dopant on the bonding of TiAl/TiO<sub>2</sub> interface. *Intermetallics* **2014**, *49*, 1–6. [[CrossRef](#)]
20. Wang, B.; Dai, J.; Wu, X.; Song, Y.; Yang, R. First-principles study of the bonding characteristics of TiAl(111)/Al<sub>2</sub>O<sub>3</sub>(0001) interface. *Intermetallics* **2015**, *60*, 58–65. [[CrossRef](#)]
21. Li, Y.; Dai, J.; Song, Y. Research progress of first principles studies on oxidation behaviors of Ti-Al alloys and alloying influence. *Metals* **2021**, *11*, 985. [[CrossRef](#)]
22. Li, Y.; Dai, J.H.; Song, Y. Enhancing adhesion of Al<sub>2</sub>O<sub>3</sub> scale on Ti-Al intermetallics by alloying: A first principles study. *Comput. Mater. Sci.* **2020**, *181*, 109756. [[CrossRef](#)]
23. Kulkova, S.E.; Bakulin, A.V.; Hu, Q.M.; Yang, R. Adsorption and diffusion of oxygen on γ-TiAl(001) and (100) surfaces. *Comput. Mater. Sci.* **2015**, *97*, 55–63. [[CrossRef](#)]
24. Bakulin, A.V.; Latyshev, A.M.; Kulkova, S.E. Absorption and diffusion of oxygen in the Ti<sub>3</sub>Al alloy. *J. Exp. Theor. Phys.* **2017**, *125*, 138–147. [[CrossRef](#)]
25. Bakulin, A.V.; Kulkov, S.S.; Kulkova, S.E. Diffusion properties of oxygen in the γ-TiAl alloy. *J. Exp. Theor. Phys.* **2020**, *130*, 579–590. [[CrossRef](#)]
26. Bakulin, A.V.; Kulkov, S.S.; Kulkova, S.E. Adhesion properties of clean and doped Ti<sub>3</sub>Al/Al<sub>2</sub>O<sub>3</sub> interface. *Appl. Surf. Sci.* **2021**, *536*, 147639. [[CrossRef](#)]

27. Bakulin, A.V.; Kulkov, S.S.; Kulkova, S.E.; Hocker, S.; Schmauder, S. First principles study of bonding mechanisms at the TiAl/TiO<sub>2</sub> interface. *Metals* **2020**, *10*, 1298. [[CrossRef](#)]
28. Bakulin, A.V.; Kulkova, S.E. Effect of impurities on the formation energy of point defects in the  $\gamma$ -TiAl alloy. *J. Exp. Theor. Phys.* **2018**, *127*, 1046–1058. [[CrossRef](#)]
29. Jiang, H.; Wang, Z.; Ma, W.; Feng, X.; Dong, Z.; Zhang, L.; Liu, Y. Effects of Nb and Si on high temperature oxidation of TiAl. *Trans. Nonferrous Met. Soc. China* **2008**, *18*, 512–517. [[CrossRef](#)]
30. Li, X.Y.; Taniguchi, S.; Matsunaga, Y.; Nakagawa, K.; Fujita, K. Influence of siliconizing on the oxidation behavior of a  $\gamma$ -TiAl based alloy. *Intermetallics* **2003**, *11*, 143–150. [[CrossRef](#)]
31. Riley, D.P.; Oliver, C.P.; Kisi, E.H. In-situ neutron diffraction of titanium silicide, Ti<sub>5</sub>Si<sub>3</sub>, during self-propagating high-temperature synthesis (SHS). *Intermetallics* **2006**, *14*, 33–38. [[CrossRef](#)]
32. Shon, I.J.; Kim, H.C.; Rho, D.H.; Munir, Z.A. Simultaneous synthesis and densification of Ti<sub>5</sub>Si<sub>3</sub> and Ti<sub>5</sub>Si<sub>3</sub>-20 vol% ZrO<sub>2</sub> composites by field-activated and pressure-assisted combustion. *Mater. Sci. Eng. A* **1999**, *269*, 129–135. [[CrossRef](#)]
33. Yan, W.; Dai, L.; Gui, C. In situ synthesis and hardness of TiC/Ti<sub>5</sub>Si<sub>3</sub> composites on Ti-5Al-2.5Sn substrates by gas tungsten arc welding. *Int. J. Miner. Metall. Mater.* **2013**, *20*, 284–289. [[CrossRef](#)]
34. Lee, D.B.; Kim, D.J. High-temperature oxidation of TiN-Ti<sub>5</sub>Si<sub>3</sub> composites prepared by polymer pyrolysis. *Oxid. Met.* **2007**, *67*, 39–49. [[CrossRef](#)]
35. Tang, Z.; Williams, J.J.; Thom, A.J.; Akinc, M. High temperature oxidation behavior of Ti<sub>5</sub>Si<sub>3</sub>-based intermetallics. *Intermetallics* **2008**, *16*, 1118–1124. [[CrossRef](#)]
36. Swadźba, R.; Swadźba, L.; Mendala, B.; Witala, B.; Tracz, J.; Marugi, K.; Pyclik, Ł. Characterization of Si-aluminide coating and oxide scale microstructure formed on  $\gamma$ -TiAl alloy during long-term oxidation at 950 °C. *Intermetallics* **2017**, *87*, 81–89. [[CrossRef](#)]
37. Palmero, P. Structural ceramic nanocomposites: A review of properties and powders' synthesis methods. *Nanomaterials* **2015**, *5*, 656–696. [[CrossRef](#)] [[PubMed](#)]
38. Huang, J.; Zhao, F.; Cui, X.; Wang, J.; Xiong, T. Long-term oxidation behavior of silicon-aluminizing coating with an in-situ formed Ti<sub>5</sub>Si<sub>3</sub> diffusion barrier on  $\gamma$ -TiAl alloy. *Appl. Surf. Sci.* **2022**, *582*, 152444. [[CrossRef](#)]
39. Blöchl, P.E. Projector augmented-wave method. *Phys. Rev. B* **1994**, *50*, 17953–17979. [[CrossRef](#)]
40. Kresse, G.; Joubert, J. From ultrasoft pseudopotentials to the projector augmented-wave method. *Phys. Rev. B* **1999**, *59*, 1758–1775. [[CrossRef](#)]
41. Perdew, J.P.; Burke, K.; Ernzerhof, M. Generalized gradient approximation made simple. *Phys. Rev. Lett.* **1996**, *77*, 3865–3868. [[CrossRef](#)]
42. Monkhorst, H.J.; Pack, J.D. Special points for Brillouin-zone integrations. *Phys. Rev. B* **1976**, *13*, 5188–5192. [[CrossRef](#)]
43. Kematick, R.J.; Myers, C.E. Thermodynamics of the phase formation of the titanium silicides. *Chem. Mater.* **1996**, *8*, 287–291. [[CrossRef](#)]
44. Meschel, S.V.; Kleppa, O.J. Standard enthalpies of formation of some 3d transition metal silicides by high temperature direct synthesis calorimetry. *J. Alloys Compd.* **1998**, *267*, 128–135. [[CrossRef](#)]
45. Robins, D.A.; Jenkins, I. The heats of formation of some transition metal silicides. *Acta Metall.* **1955**, *3*, 598–604. [[CrossRef](#)]
46. Colinet, C.; Tedenac, J.C. Structural stability of intermetallic phases in the Si-Ti system. Point defects and chemical potentials in D8<sub>8</sub>-Si<sub>3</sub>Ti<sub>5</sub> phase. *Intermetallics* **2010**, *18*, 1444–1454. [[CrossRef](#)]
47. Poletaev, D.O.; Aksyonov, D.A.; Lipnitskii, A.G. Evolutionary search for new compounds in the Ti-Si system. *Calphad* **2020**, *71*, 102201. [[CrossRef](#)]
48. Zhang, P.F.; Li, Y.X.; Bai, P.K. First principles study of Ti<sub>5</sub>Si<sub>3</sub> intermetallic compounds with Cu additions: Elastic properties and electronic structure. *IOP Conf. Ser. Mater. Sci. Eng.* **2017**, *284*, 012013. [[CrossRef](#)]
49. Bakulin, A.V.; Kulkova, S.E.; Hu, Q.M.; Yang, R. Theoretical study of oxygen sorption and diffusion in the volume and on the surface of a  $\gamma$ -TiAl alloy. *J. Exp. Theor. Phys.* **2015**, *120*, 257–267. [[CrossRef](#)]
50. Latyshev, A.M.; Bakulin, A.V.; Kulkova, S.E. Adsorption of oxygen on low-index surfaces of Ti<sub>3</sub>Al alloy. *Phys. Solid State* **2017**, *59*, 1852–1866. [[CrossRef](#)]
51. Villars, P.; Calvert, L.D. *Pearson's Handbook of Crystallographic Data for Intermetallic Phases*; ASM: Metals Park, OH, USA, 1985.
52. Yurov, V.M.; Eremin, E.N.; Guchenko, S.A.; Laurinas, V.C. Surface Energy and Thickness of Surface Layer of Atomic-Smooth Metals Silicides. *AIP Conf. Proc.* **2019**, *2141*, 040024. [[CrossRef](#)]
53. Sunagawa, I. *Crystals: Growth, Morphology and Perfection*; Cambridge University Press: Cambridge, UK, 2005.
54. Wang, X.; Jie, J.; Liu, S.; Dong, Z.; Yin, G.; Li, T. Growth mechanism of primary Ti<sub>5</sub>Si<sub>3</sub> phases in special brasses and their effect on wear resistance. *J. Mater. Sci. Technol.* **2021**, *61*, 138–146. [[CrossRef](#)]
55. Abba, A.; Galerie, A.; Caillet, M. High-temperature oxidation of titanium silicide coatings on titanium. *Oxid. Met.* **1982**, *17*, 43–54. [[CrossRef](#)]
56. Wei, L.J.; Guo, J.X.; Dai, X.H.; Wang, Y.L.; Liu, B.T. Adsorption and dissociation of O<sub>2</sub> on Ti<sub>3</sub>Al(0001) studied by first-principles. *Surf. Rev. Lett.* **2015**, *22*, 1550053. [[CrossRef](#)]
57. Loffreda, D. Theoretical insight of adsorption thermodynamics of multifunctional molecules on metal surfaces. *Surf. Sci.* **2006**, *600*, 2103–2122. [[CrossRef](#)]

- 
58. Manz, T.A.; Limas, N.G. Introducing DDEC6 atomic population analysis: Part 1. Charge partitioning theory and methodology. *RSC Adv.* **2016**, *6*, 47771–47801. [[CrossRef](#)]
  59. Manz, T.A. Introducing DDEC6 atomic population analysis: Part 3. Comprehensive method to compute bond orders. *RSC Adv.* **2017**, *7*, 45552–45581. [[CrossRef](#)]